

Article

Analysis and Experimental Validation of Single-Phase Cascaded Boost AC–AC Converter with High Voltage Gain

Dina S. M. Osheba ¹, Sayed M. Ahmed ^{1,2,*} and Azza E. Lashine ¹

¹ Department of Electrical Engineering, Faculty of Engineering, Menoufia University, Shebin El-Kom 32511, Egypt

² Department of Industrial Technology, Faculty of Technological Industry and Energy, Delta Technological University, Quesna 32631, Egypt

* Correspondence: sayed.mohamed45@sh-eng.menofia.edu.eg

Abstract: This article presents a single-phase cascaded AC–AC converter with boosting capability for power-quality issues. A high voltage gain can be obtained based on the number of cascaded units. The basic construction of one unit in the cascaded connection requires only two four-quadrant switches with a low-voltage rating. The performance features for the topology are a unity power factor that is close to unity on the input side, high steady-state performance, and fast dynamic response. The operation modes and mathematical model for the topology are presented. An appropriate PI-based control method/strategy is created, so the converter may continue to run while attaining the desired voltage gain, even if one of the cascaded units fails. The control circuit's ability to maintain the continuity of matching the input current waveform with the input voltage waveform allows a decrease in the THD with different operating conditions. Moreover, the ability to solve a dead time problem carried out by the control circuit leads to a reduction in voltage stress. The effectiveness and robustness of the proposed technique were demonstrated via a computer simulation using MATLAB/Simulink. Moreover, an experimental setup for the system was built in the laboratory to validate the practicability of the system, which was tested under different conditions. The good agreement obtained between the theoretical and experimental results endorses the validity of the designed circuit.

Keywords: AC–AC converter; four-quadrant switches; high voltage gain



Citation: Osheba, D.S.M.; Ahmed, S.M.; Lashine, A.E. Analysis and Experimental Validation of Single-Phase Cascaded Boost AC–AC Converter with High Voltage Gain. *Sustainability* **2023**, *15*, 3353. <https://doi.org/10.3390/su15043353>

Academic Editor: Mohamed Abdelrahem

Received: 30 November 2022

Revised: 9 February 2023

Accepted: 10 February 2023

Published: 12 February 2023



Copyright: © 2023 by the authors. Licensee MDPI, Basel, Switzerland. This article is an open access article distributed under the terms and conditions of the Creative Commons Attribution (CC BY) license (<https://creativecommons.org/licenses/by/4.0/>).

1. Introduction

Current industrial growth has resulted in considerable power-quality challenges, particularly with regard to voltage profile and harmonic distortion [1]. Among the aforementioned issues, utility voltage sag/swell is one of the most common problems, particularly from the perspective of the ultimate customer, with regard to sensitive loads linked to the grid [2]. In AC power systems, AC voltage controllers are used to solve many voltage problems [3], by injecting AC voltage through a series-connected transformer. This stresses the extreme need for applications that cure the issues associated with the power-quality problem. As a result, end-users must employ power-conditioning devices and controllers to deal with such issues, for the safe and proper operation of their equipment. AC-to-AC power conversion, utilizing dependable and efficient converters capable of meeting stringent power-quality requirements, remains a challenge in many industrial applications such as variable-speed motors, electric heaters, AC voltage regulators, etc. [4,5].

AC–AC converters are divided into three main categories. The first type is AC–DC–AC indirect converters, which are applicable for the variable adjustment of the amplitude, phase, and frequency of the output AC voltage with a constant DC-link. The power conversion consists of two stages (AC to DC and DC to AC) and requires a large, short-lasting electrolytic capacitor on the DC connection [6–9]. The second type is matrix converters,

which are used in applications where both the voltage magnitude and frequency must be changeable [10–13]. A traditional matrix converter allows for varying the output frequency and voltage at the expense of a more complex modulation technique and a higher number of switches. The third type is direct AC-to-AC converters, which can provide single-stage AC power conversion, eliminating the DC-link capacitor [14–17]. They provide several benefits, such as easy circuits' implementation, a simpler control algorithm, a compact size, and a reduced total cost [18–20].

Cascaded AC–AC converters are commonly used [21–24] and are considered a suitable option for medium- and high-voltage systems. Cascaded converters have been recognized as an attractive topology in high-voltage direct current (HVDC) transmission, solid-state transformers (SSTs), a microgrid, and wind farm (WF) systems, due to their many merits. They have many features that attract researchers to work in this field, as follows: Firstly, they can be used to obtain high-gain output voltages using low-voltage rating switching devices at low switching frequencies. Secondly, they produce AC output voltages with higher power-quality waveforms.

A cascaded converter based on the conventional AC/AC converter has a commutation problem for each unit. This has not been well-supported with phase-shift PWM control [25].

The main disadvantage of cascaded topologies [22–24] is their use of a buck converter, which leads to an increase in the number of units required to obtain a high voltage; thus, the cost and size are high. The cascaded three-level AC/AC direct converter in [22] used six bidirectional power switches. The load was not connected to the supply in any mode; therefore, it is suitable for low-power applications. Moreover, the power factor (PF) for inductive loads is not improved. In [23], a single-phase cascaded multilevel AC–AC converter that operates with pulse-width modulation (PWM) was proposed. This converter works without commutation problems but uses extra-coupled inductors for each unit, to obtain a high gain. A coupled inductor limits the circulating currents only and does not serve as a filter inductor. Extra-coupled inductors lead to a high cost and large weight.

A cascaded dual-buck AC–AC converter with a reduced number of inductors is presented in [24]. It reduces the number of coupled inductors in each unit and uses a phase-shift control to solve the commutation problems. The operation modes for a cascaded connection rise with the unit's increasing number, leading to a complicated phase-shift control circuit.

In [25], a cascaded dual-buck AC–AC topology is proposed with fewer inductors to obtain high output voltages and decrease the converter cost and volume. This type operates with low voltage-rating devices, MOSFETs, and disables their body diodes that may be damaged. In addition, the control system is very complicated due to the complexity of its operation states.

In this article, a single-phase cascaded boost AC/AC converter is introduced, in which each unit has its own AC power supply and can be connected to (n) units to obtain high output voltages. This system has many advantages, such as using standard low-voltage rating semiconductor modules and a simple structure for each unit. Furthermore, each unit has boosting capability; consequently, it obtains a high voltage with fewer units compared to previous topologies. Compared to the phase-shift control technique, a simple control technique is used to solve the commutation problems. In addition, the THD of the input current and the output voltage are reduced, and the power factor is close to unity.

A theoretical study was carried out by building a mathematical model of the proposed technique and investigating its operation modes. Furthermore, a MATLAB/Simulink model was built using four units and three units. Finally, the actual performance was tested by a laboratory setup via DSP1104 using two units and three units.

This paper is organized as follows: A description of the proposed system is discussed in Section 2 as well as the control circuit for a cascaded AC boost converter. The operation modes, mathematical analysis, and average state-space representation with a Bode plot drawing are discussed in Section 3. Section 4 illustrates the simulated results for the proposed system under the steady-state and transient conditions. A prototype of a high-gain

cascade AC–AC converter was built using two units, and the experimental results are presented in Section 5. Section 6 presents the comparison between the simulated and experimental results using three units. Finally, the conclusions are highlighted in Section 7.

The contributions of this paper are as follows:

1. A high-voltage-gain cascaded AC-to-AC boost converter is presented, which utilized low-voltage-rating semiconductor devices and multiple cascaded boost units.
2. The output voltage waveform was found to be a sine wave with low harmonics, and the robustness of the control system was confirmed through a case study in which a fault occurred at one unit.
3. The control circuit's ability to maintain the continuity of the output voltage after a fault occurs was confirmed.
4. The proposed circuit was verified through both the simulated and experimental results, which demonstrated an excellent dynamic response with a continuous input current and a power factor close to unity.

2. Power and Control Circuit

Figure 1 shows the proposed cascaded AC–AC boost voltage regulator. In this circuit, a boost AC–AC converter with two bidirectional switches S_{1n} , S_{2n} is used. An input boost inductor L_{s1} lies between the AC source and the switch S_{1n} . To achieve an output voltage greater than the input voltage, several units of this converter can be used in a series. A multi-winding low frequency 50 Hz transformer is used to create the isolated input voltages (v_{s1} , v_{s2} , v_{s3} , and v_{sn}) [24]. In the proposed system, it is possible to obtain a high voltage gain with fewer units because the basic unit has a step-up gain. The isolation between one stage and the other stages, in the case of the failure of the semiconductors, occurs through the two solid-state relays (SSR). The first switch is placed between the source and the boost coil and is activated when the circuit is operating normally, while the second switch is placed at the ends of the capacitor and is activated when the unit has a malfunction.

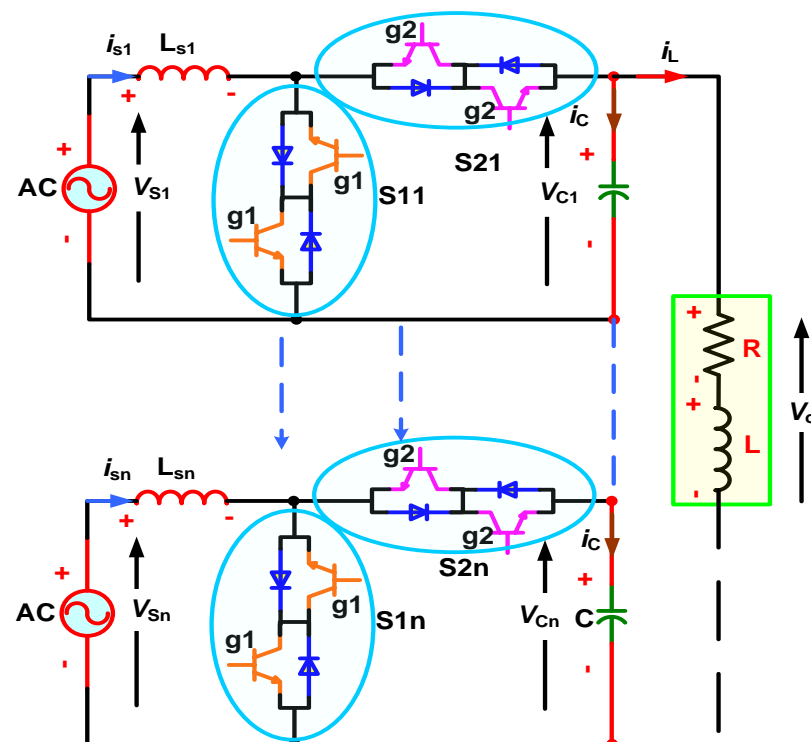


Figure 1. Proposed cascaded boost AC–AC converter for n units.

Various control approaches for AC–AC power converters are documented in the literature [18,26]. PI-based techniques are considered the most applied methods for AC

power-conversion systems. In this work, a PI-based hysteresis control method is designed. Figure 2 shows the block diagram of the developed control method. A PI controller is used for the outer loop, which is the voltage-control loop. After generating the reference current command from the PI controller, a hysteresis controller is used to generate the pulses for the switches. The load voltage requirements are used to determine the voltage reference signal V_o^* . A proportional integral (PI) controller receives the error signal. The command currents I_s^* are then calculated by multiplying the controller output by the supply voltages/unit value. The supply current i_s is compared with the demand currents. The error signal from the comparator is processed by a hysteresis controller. As shown in Figure 2, the hysteresis controller output is employed as the input for the SR flip-flop to contribute to solving the commutation problem. As a result, the SR flip-flop output (Q) is used to generate the signal pulse for S_{1n} , and NOT (Q) is used to generate the signal pulse for S_{2n} . The supply current is controlled to follow the current command, which follows the supply voltage in its waveform and follows the reference voltage in its magnitude. This control strategy ensures that the input power factor is nearly kept close to a unity value, and the output voltage becomes equal to the reference voltage.

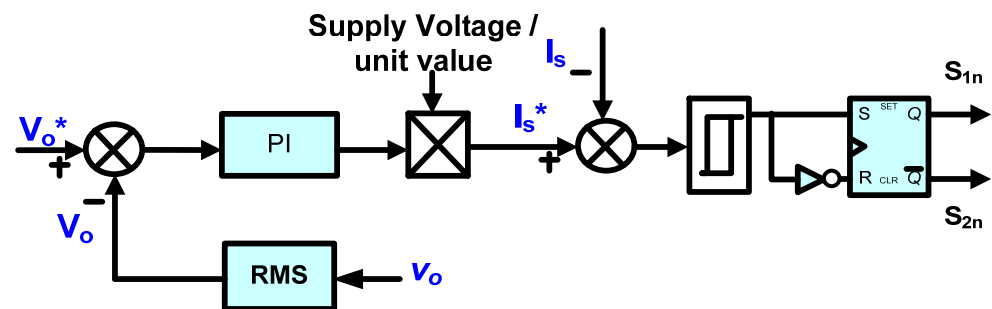


Figure 2. Block diagram of the proposed control strategy.

3. Mathematical Analysis and Operation Modes

In this section, the mathematical analysis for the converter is presented. There are two modes of operation for the cascaded boost AC–AC converter.

3.1. Mode 1

In this mode, the bidirectional switch S_{1n} is turned off, while the bidirectional switch S_{2n} is turned on. The power delivered to the load and capacitor is equal to the energy stored in the inductors and the supplies' voltage, until the current supply reduces to the lower band of the hysteresis controller. Figure 3 depicts mode 1 during the positive half cycle for the proposed system, in which switch S_{2n} is turned on. The complementary switch of S_{2n} is turned on during the negative half cycle, as shown in Figure 4. The simplified equivalent circuit for mode 1 is shown in Figure 5.

The input voltage equations for mode 1 in Figure 5 can be represented as

$$v_{sn} = V_{sn} \sin(\omega t), \quad (1)$$

$$v_s = v_{s1} = v_{s2} = v_{s3} = \dots v_{sn}, \quad (2)$$

where v_s is the instantaneous supply voltage, V_{sn} is the maximum supply voltage for unit n , v_n is the instantaneous supply voltage for unit n , L_{sn} is the boost inductor for unit n , and n is the number of the units (1, 2, and 3 . . . , n). Referring to the equivalent circuits of Figure 5 for mode 1, by applying Kirchhoff's voltage law to achieve Equations (3) and (4), the equations representing mode 1 can be written as

$$nv_s = ni_s r_s + n \frac{di_s}{dt} L_s + v_o \quad (3)$$

$$v_o = nv_{cn} = i_L R + L \frac{di_L}{dt} = \frac{n}{C} \int i_c dt + nv_{cno}, \tag{4}$$

$$\begin{bmatrix} \dot{i}_s \\ \dot{v}_c \end{bmatrix} = \begin{bmatrix} 0 & -\frac{1}{L_s} \\ \frac{n}{c} & -\frac{n}{cR} \end{bmatrix} \begin{bmatrix} i_s \\ v_c \end{bmatrix} + \begin{bmatrix} \frac{1}{L_s} \\ 0 \end{bmatrix} [v_s]. \tag{5}$$

where v_o is the instantaneous output voltage, v_{cn} is the voltage for a capacitor C , v_{cno} is the initial voltage for a capacitor C , i_L is the instantaneous value of the load current, and i_c is the instantaneous capacitor current.

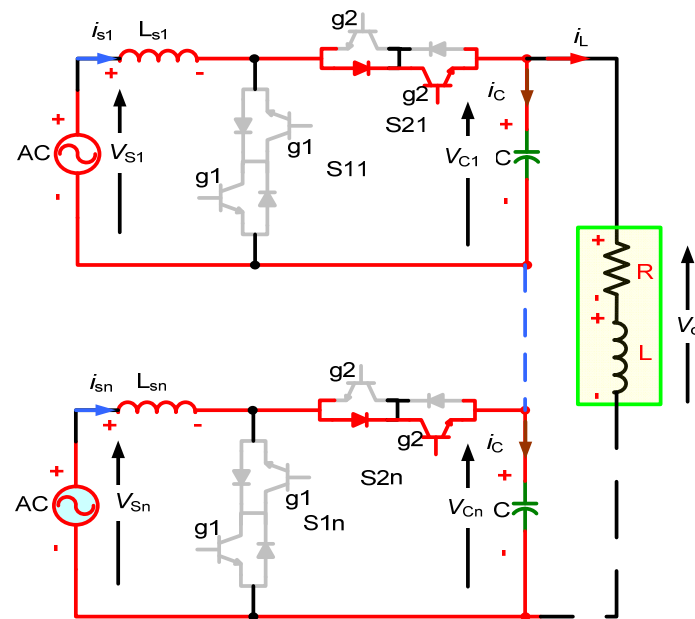


Figure 3. Mode 1 of the proposed cascaded boost AC-AC converter using (n) units during the positive half cycle.

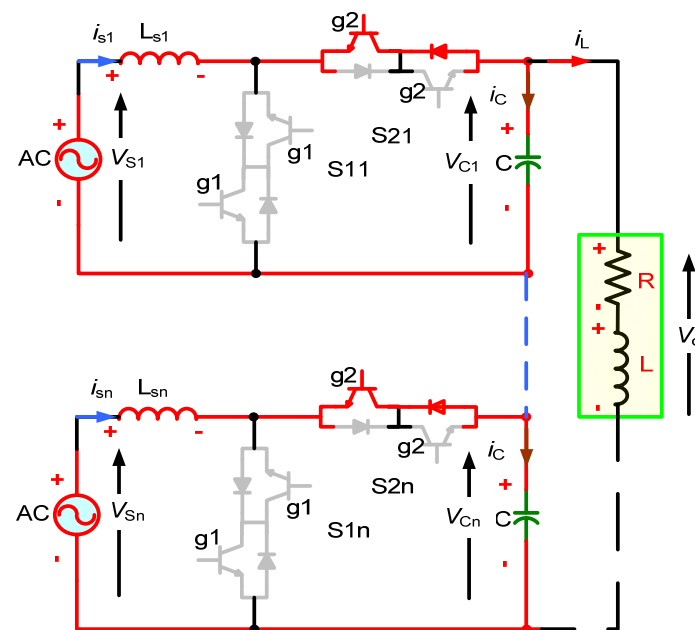


Figure 4. Mode 1 of the proposed cascaded boost AC-AC converter using (n) units during the negative half cycle.

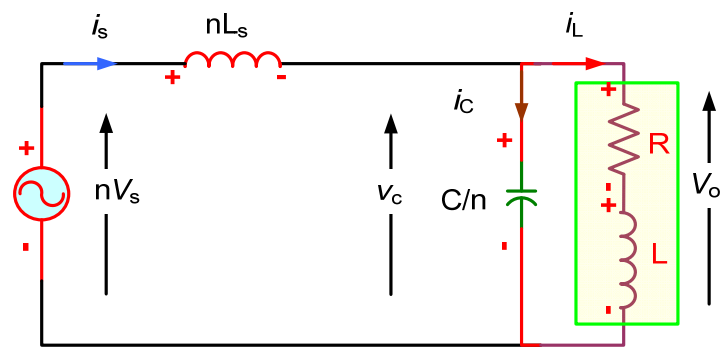


Figure 5. Equivalent circuit for mode (1).

3.2. Mode 2

The bidirectional switch S_{1n} is turned on, while the bidirectional switch S_{2n} is turned off in mode 2. The load is supplied from the sum of the energy stored in each capacitor. Moreover, the supply current (i_s) stores energy in the inductor and increases up to the upper band limit of the hysteresis reference. During the positive half cycle, the switch S_{1n} is turned on, as shown in Figure 6. The complementary switch of S_{1n} is turned on during the negative half cycle, as illustrated in Figure 7. The simplified equivalent circuit for mode 2 is shown in Figure 8. By applying Kirchhoff’s voltage law to the equivalent circuit in Figure 8, we obtain the following equations:

$$nv_s = ni_s r_s + n \frac{di_s}{dt} L_s \tag{6}$$

$$v_o = R + L \frac{di_L}{dt} = \frac{n}{C} \int i_c dt + nv_{co}, \tag{7}$$

$$i_c = -i_L. \tag{8}$$

$$\begin{bmatrix} \dot{i}_s \\ \dot{v}_c \end{bmatrix} = \begin{bmatrix} 0 & 0 \\ 0 & -\frac{n}{cR} \end{bmatrix} \begin{bmatrix} i_s \\ v_c \end{bmatrix} + \begin{bmatrix} \frac{1}{L_s} \\ 0 \end{bmatrix} [v_s]. \tag{9}$$

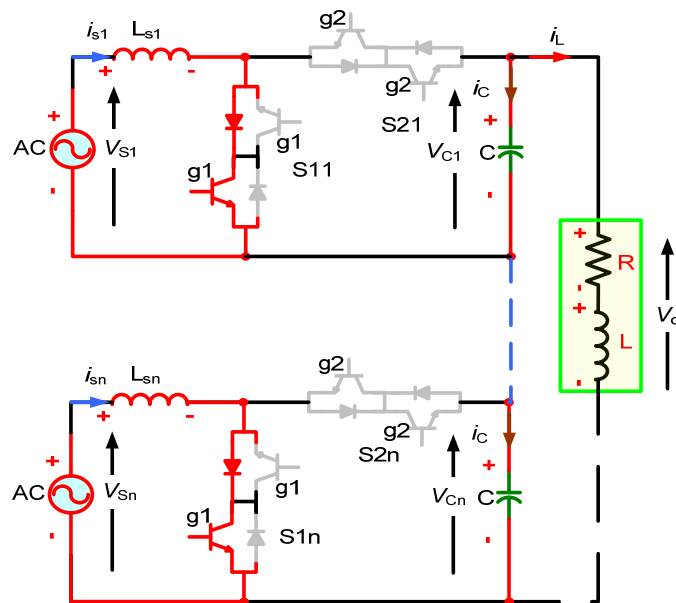


Figure 6. Mode 2 of the proposed cascaded boost AC–AC converter using (n) units during the positive half cycle.

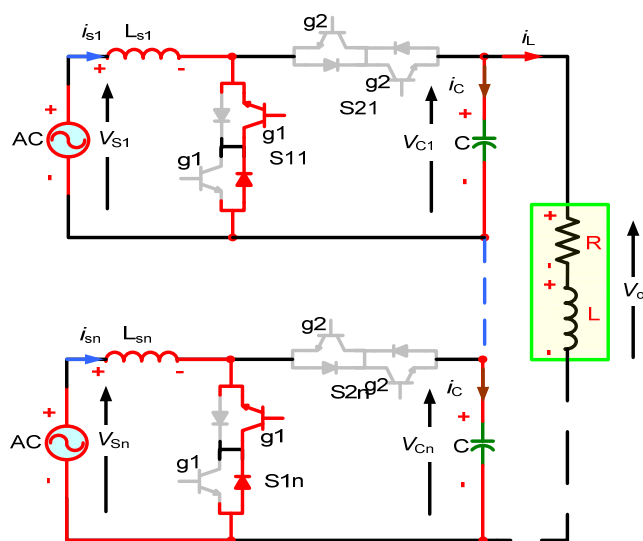


Figure 7. Mode 2 of the proposed cascaded boost AC-AC converter using (n) units during the negative half cycle.

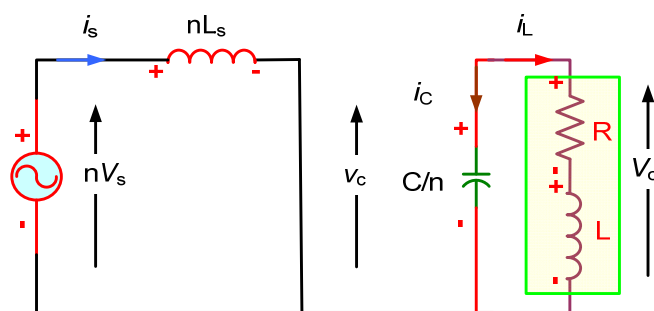


Figure 8. Equivalent circuit for mode (2).

3.3. Average State-Space Representation

The state-space representation of the cascaded AC-AC converter at operating continuous conduction modes (CCM) [27–30] can be defined in the following standard form of the state-space model.

$$\dot{X} = A * X + B * U \tag{10}$$

In mode 1, the ratio is (1-D) of the duty cycle. The standard state-space format, from Equation (5), can be written as follows:

$$\dot{X} = A_{off} * X + B_{off} * U \tag{11}$$

As for mode 2, the ratio is D of the duty of cycle, and Equation (9) can be written as follows:

$$\dot{X} = A_{on} * X + B_{on} * U \tag{12}$$

Assuming the duration period of mode 2 is D, the mode 1 duration period is 1-D to represent one cycle. Therefore, from Equations (11) and (12), by using the average technique, the overall state-space model of the converter can be written as

$$\dot{X} = [D * A_{on} + (1 - D) * A_{off}] X + [D * B_{on} + (1 - D) B_{off}] U \tag{13}$$

Equation (13) represents the average large-signal model of the state variable. Consider the case when a small signal fluctuation (*d*) happens at the initial duty ratio (*D*₀), resulting in a tiny variation (*x*) of the initial state variables (*X*₀). This may be written as follows:

$$\begin{aligned} \dot{X}_0 + \dot{x} = & \left[(D_0 + d) * A_{on} + (1 - D_0 - d) * A_{off} \right] * (X_0 + x) \\ & + \left[(D_0 + d) * B_{on} + (1 - D_0 - d) * B_{off} \right] * U \end{aligned} \quad (14)$$

Equation (14) yields the following small-signal model, which represents the dynamic characteristics of the converter when subjected to a small deviation in the duty ratio:

$$\dot{X} = A * x + F * d \quad (15)$$

where

$$A = D_0 A_{on} + (1 - D_0) A_{off} \quad (16)$$

and

$$F = [A_{on} - A_{off}] * X_0 + [B_{on} - B_{off}] * U \quad (17)$$

Equation (15) can be solved using the Laplace transform to obtain the converter transfer function:

$$\frac{x}{d} = [sI - A]^{-1} F \quad (18)$$

$$\frac{x}{d} = \frac{\begin{bmatrix} \hat{i}_s \\ \hat{v}_c \end{bmatrix}}{d} = \frac{adj[sI - A]F}{det[sI - A]}, \quad (19)$$

The TF of the converter is calculated using the MATLAB symbolic functions reduction, as follows:

$$\frac{v_c}{d} = \frac{A_1 s + A_2}{B_1 s^2 + B_2 s + B_3} = \frac{-4.0741e06 (s - 1800)}{s^2 + 3333s + 1.2e07} \quad (20)$$

Figure 9 shows the frequency response of the converter as a Bode plot fusing the dynamic model. The result reveals a nearly constant gain at low frequencies prior to the resonance frequency, followed by a gain of around 50 dB per decade at high frequencies. The positive phase shift in the phase frequency may be seen in this result. This is due to the existence of a zero in the S-plane on the right-hand side (RHS) of the system characteristic equation. As a result of these findings, the converter transfer function (TF) is referred to as a non-minimum phase system.

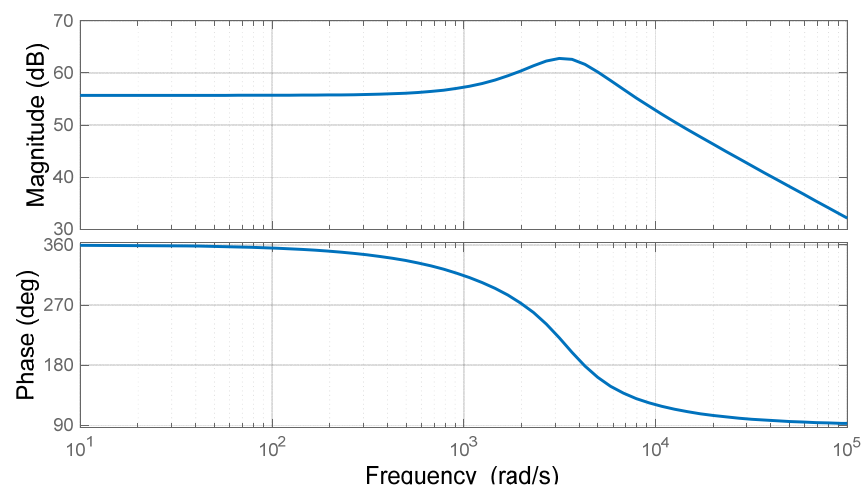


Figure 9. Bode plot diagram of the converter.

4. Simulated Results

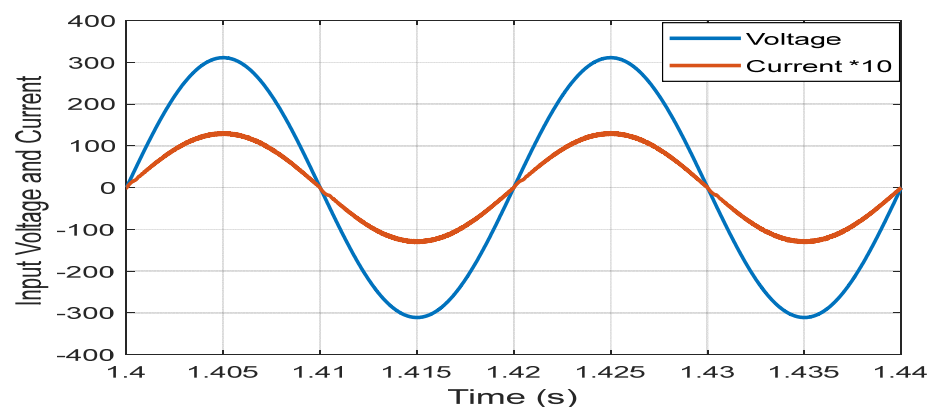
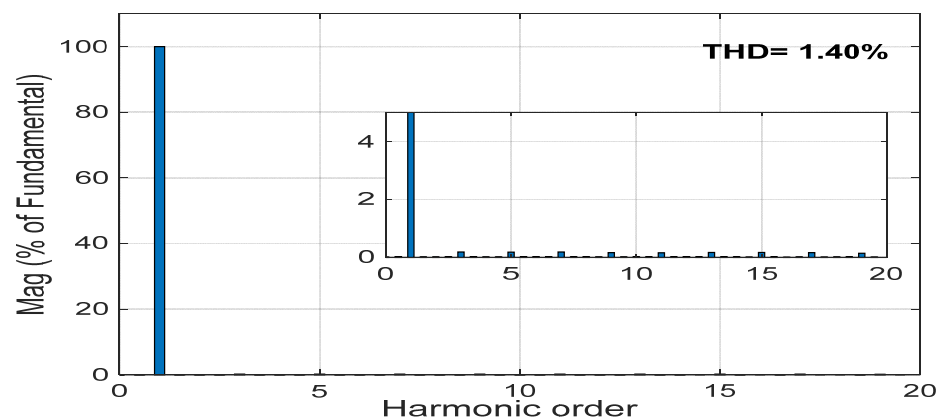
The proposed cascaded boost AC–AC converter with four units and also with three units is tested using MATLAB software. The simulated results that were obtained for the proposed system with the circuit parameters are listed in Table 1.

Table 1. Simulated parameters of the system.

Parameter	Symbol	Value
Supply phase voltage	$V_{s1} = V_{s2} = V_{sn}$	220 V
System frequency	F	50 Hz
Coil inductance	$L_{s1} = L_{s2} = \dots L_{sn} =$	15 mH
Capacitor	C_f	15 μ F
Load resistance	R	200 Ω
Load inductance	L	200 mH

4.1. Steady-State Results Using Four Units

The reference output voltage is set at 1600 V. Figure 10 shows the supply phase voltage (v_{s1}) and current (i_{s1}). It is clear that the input current is sinusoidal and in phase with the supply voltage, so the supply has a power factor close to unity. From Figure 11, it is obvious that the total harmonic distortion (THD) of the supply current is equal to 1.4%, which meets the IEEE standards, and a small graph illustrates the harmonics values with the order of the harmonics of the input current. Figure 12 shows the output voltage of the converter, which is nearly sinusoidal with a THD of 1.12, as shown in Figure 13. The small graph in Figure 12 zooms in on two cycles of the output voltage at 1 s, while Figure 13 focuses on the harmonics values with the harmonics order of the output voltage. Figure 14 shows the output current, which is sinusoidal. The inductor current with a signal pulse of S_{1n} is demonstrated in Figure 15, and the switching frequency of supply current varies between nearly 1 and 12 KHz. The voltage and current across the switch (S_{1n}) are displayed in Figure 16.

**Figure 10.** Supply voltage and current.**Figure 11.** THD of the supply current.

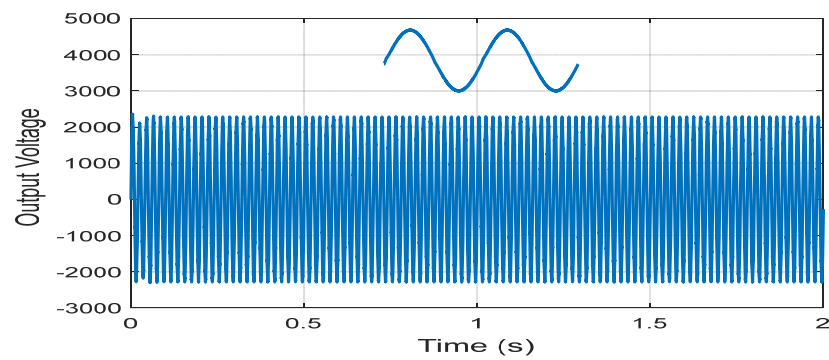


Figure 12. Output voltage.

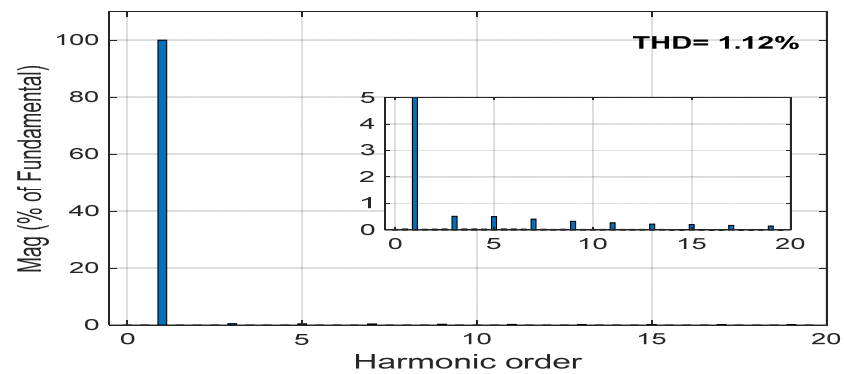


Figure 13. THD of the output voltage.

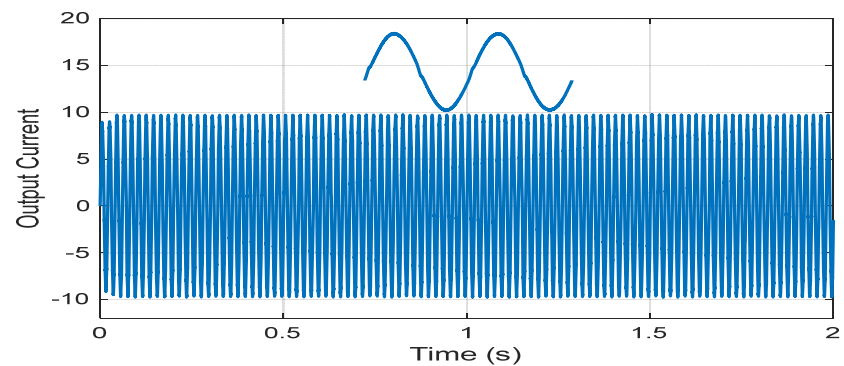


Figure 14. Output current.

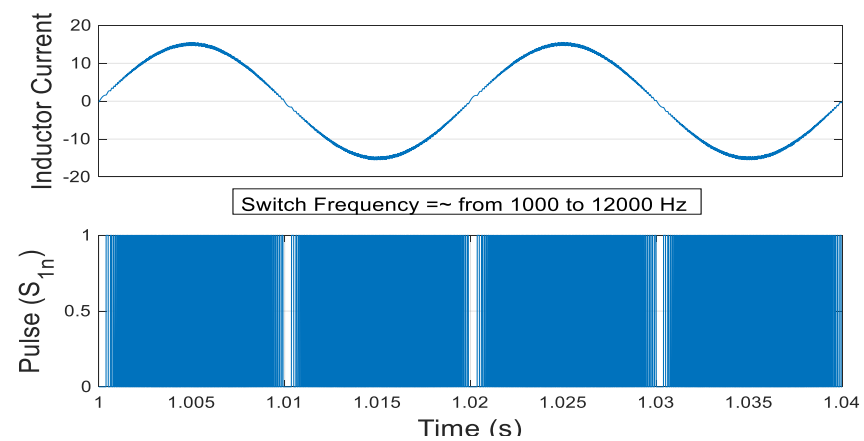


Figure 15. The input current with the signal pulse of (S_{1n}) .

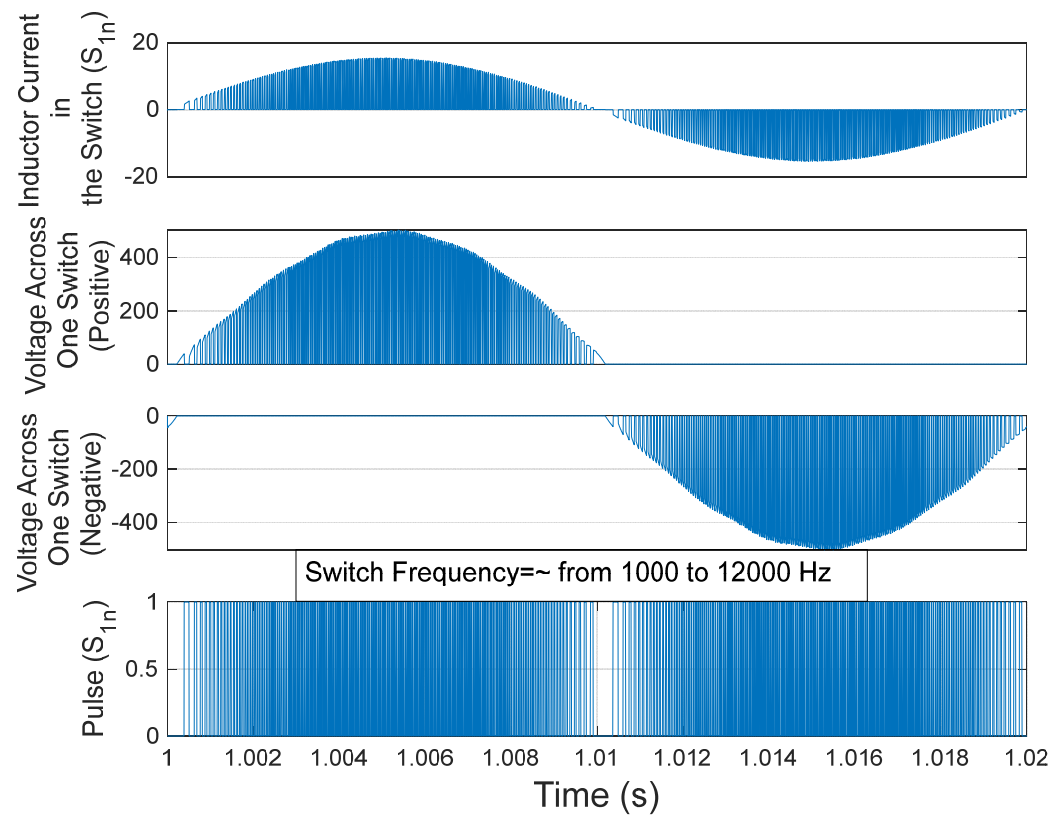


Figure 16. The current and voltage across switch (S_{1n}) with the signal pulse.

4.2. Transient Results Using Four Units

A transient study is carried out using three states to identify the control system’s reliability and responsiveness. The first case is when the load has been increased by 30% for 1 sec and is then returned to the rated value for 2 s. The load voltage (V_o) rapidly tracks the reference value (1400 V), which indicate the reliability of the system, as shown in Figure 17. Figure 18 shows the response of the load voltage during the load change. Figure 19 shows the output voltage of the converter when the load changes by 50%. The output current of the converter is shown in Figure 20, with a 50% variation in load.

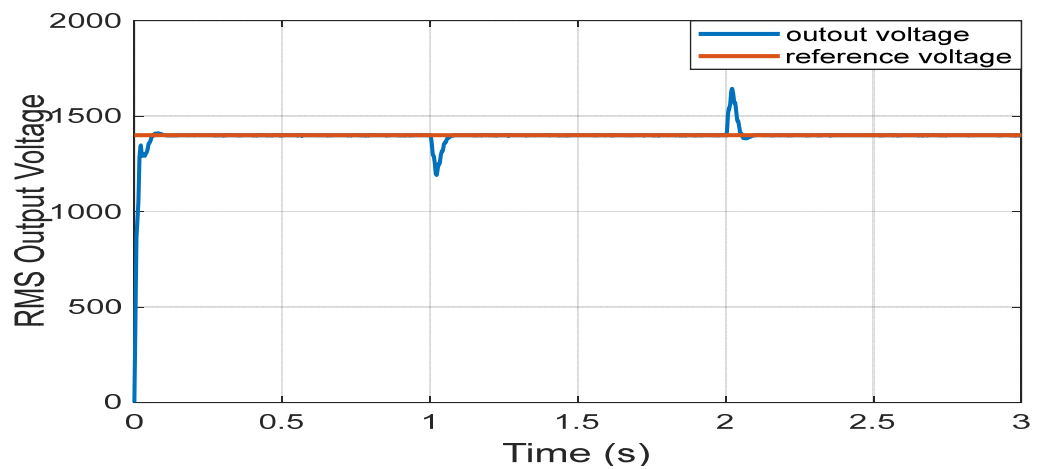


Figure 17. RMS output voltage with reference.

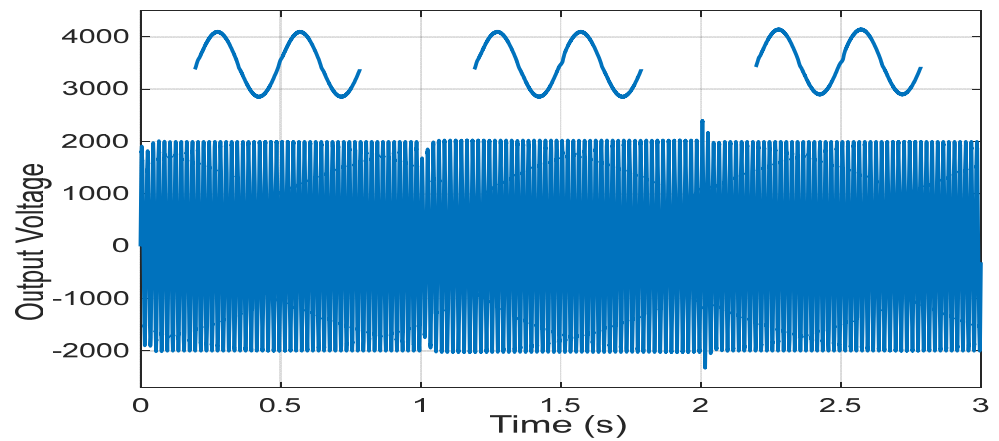


Figure 18. Output voltage during load change.

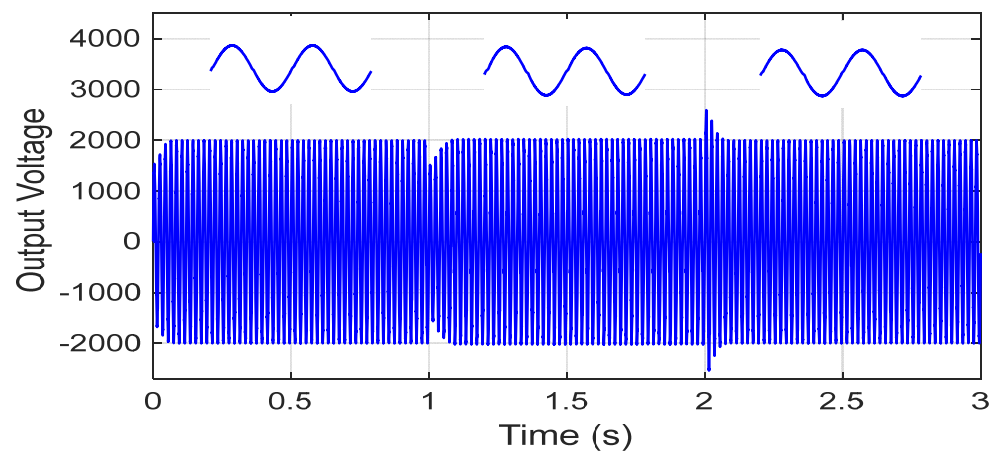


Figure 19. Output voltage when load changes by 50%.

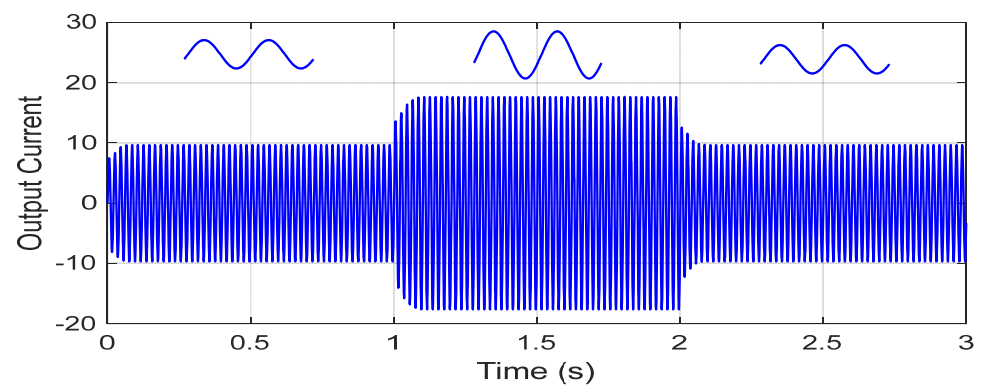


Figure 20. Output current when load changes by 50%.

The second case is when the reference voltage changes through a step change from 1200 V to 1600 V and then back to 1200 V, which occurred for 1 s. It is clear from Figure 21 that the output voltage rapidly tracks the reference one, and the instantaneous output voltages during this change and for one unit are shown in Figures 22 and 23, respectively. Thus, the output voltages are nearly sinusoidal and meet the power-quality requirements for the loads.

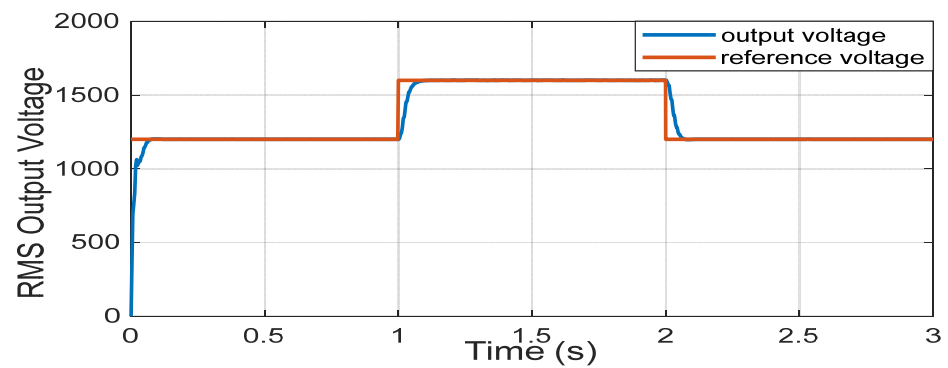


Figure 21. RMS load voltage with reference.

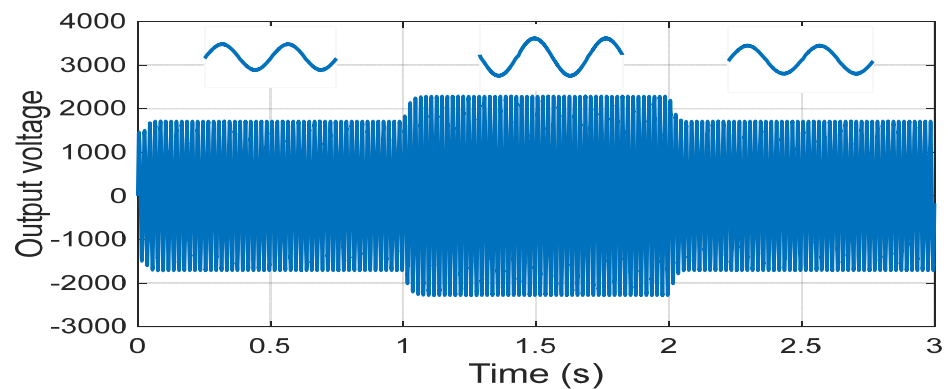


Figure 22. Single-phase load voltage.

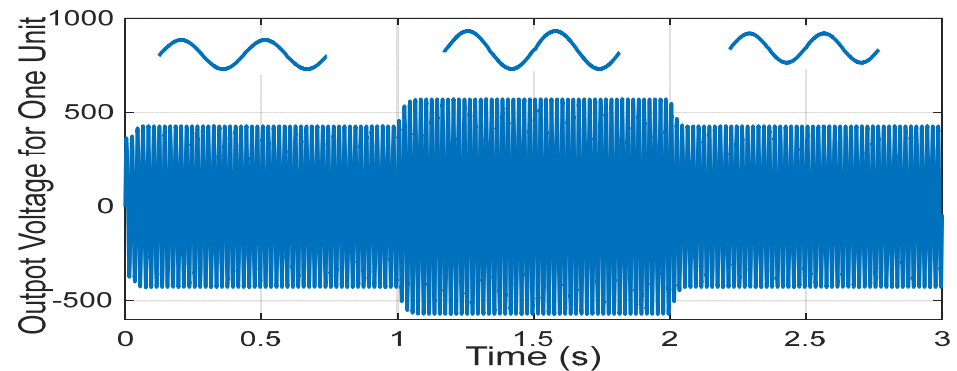


Figure 23. Output voltage for one unit.

The third case is when a study is completed to show the operation of the converter when one unit fails. From 1 s to 2 s, one of the units stops working. The faulty unit is isolated when the control circuit detects that the current input is more than $(IS^* + 2H)$ or less than $(IS^* - 2H)$. If one or both of the two conditions are satisfied, the control circuit turns off the relay (SSR) located between the source and the boost coil, while the relay across the capacitor is turned on. Figure 24 shows the RMS value of the output voltage, while the instantaneous value of the output voltage is shown in Figure 25. It is evident that the control system can keep the output voltage at the desired level, whether all units are operational or one of them is malfunctioning. The one-unit output voltage is shown in Figures 26 and 27. In Figure 26, the output voltage for the unit that fails to work is illustrated; the output voltage for this unit drops to zero from 1 s up to 2 s. Figure 27 shows the output voltage for each of the other three units individually. It is clear that when a problem occurs, each unit increases its output voltage to achieve a constant overall output voltage.

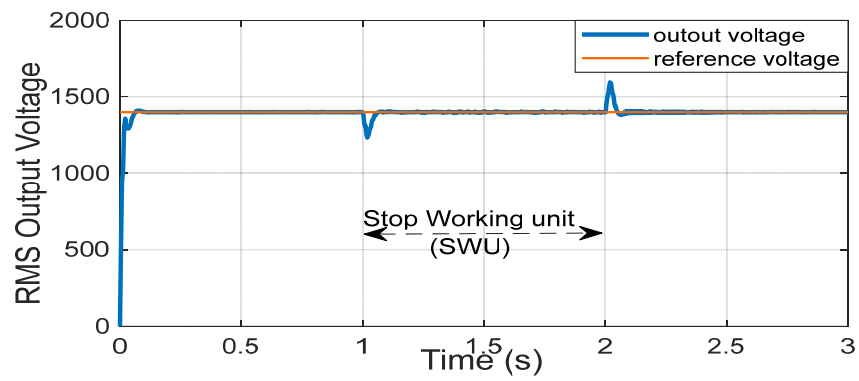


Figure 24. RMS of output voltage with reference.

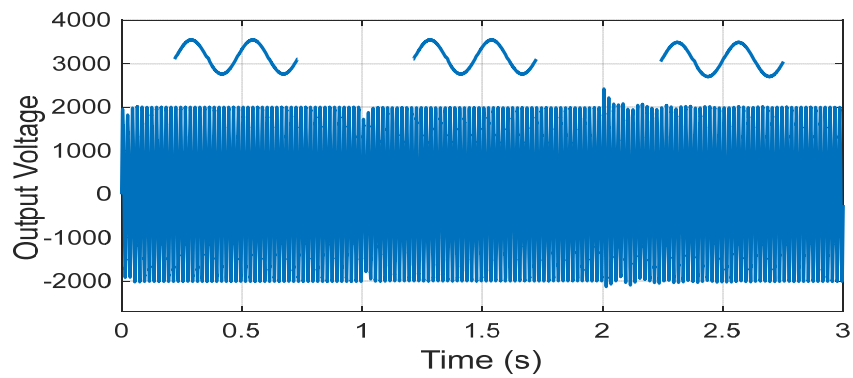


Figure 25. Single-phase load voltage.

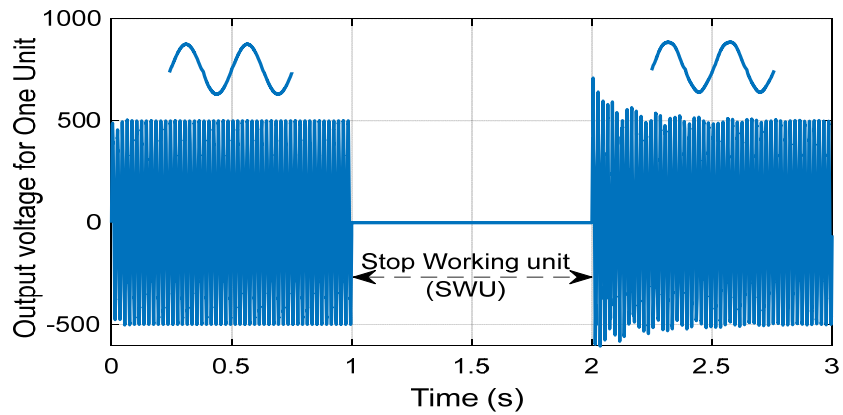


Figure 26. Output voltage of stop working unit (SWU).

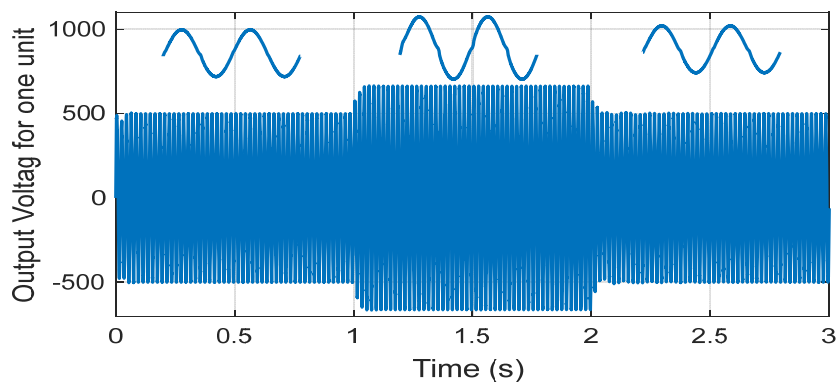


Figure 27. Output voltage for one unit.

The proposed converter is then compared to previous topologies, as shown in Table 2. The proposed converter has fewer components and a higher load voltage and output voltage gain at $D = 0.5$.

Table 2. Comparison of the proposed converter with previous topologies.

Topology	No. of Units	Inductors	Coupled Inductors	Capacitors	Switches	Diodes	Total Components	Voltage Gain (V_o/V_{in})	Output Voltage Gain	Function Unit
24	2	2	2	4	8	8	24	$2D$	$1 * V_{in}$	buck
25	3	-	-	2	12	12	26	$(D + D') / (2(1 - D))$	$1 * V_{in}$	buck
26	4	1	8	8	16	16	49	$4D$	$2 * V_{in}$	buck
27	4	1	8	9	16	16	50	$n * D$	$2 * V_{in}$	buck
Proposed	4	4	-	4	16	-	32	$n / (1 - D)$	$8 * V_{in}$	boost

5. Experimental Results

A laboratory prototype was built in order to experimentally study the performance of the converter. The experimental setup is depicted in Figure 28 as a block diagram. Figure 29 shows the actual picture of the experimental system. A single-phase multi-winding transformer was used to supply the voltage utilized to create the isolated input voltages. The prototype cascaded boost AC–AC converter was implemented using two bidirectional powers switches (IGBTs-CM100DY-24H). A solid-state relay (SSR–60 VA) was used to isolate the faulty unit. The output voltage was built up according to the required voltage (the reference value). The main components of the system are shown in Figure 29. The system parameters for the experimental investigation are listed in Table 3. A DSPACE (DS1104) controlled board was used as a real-time controller. Between the DSPACE board and the IGBT, a pulse amplifier circuit was utilized to create pulses of about 15 V for effective IGBT switching. The separate single-phase supply voltages, supply currents, and load voltage were measured using voltage and current sensors, and their signals were sent to the DSPACE control board via the A/D converter ports. All the schemes in the cascaded boost AC–AC converter were realized using a DSPACE board DS-1104, which is based on a 32-bit floating-point DSP TMS320C31. The board was combined with a fixed-point 16-bit TMS320P14 DSPACE as a slave processor, as illustrated in Figure 28. This DSPACE board system experiments with the proposed control algorithms. The DSPACE makes it easier to collect and numerically output experimental waveforms per sample.

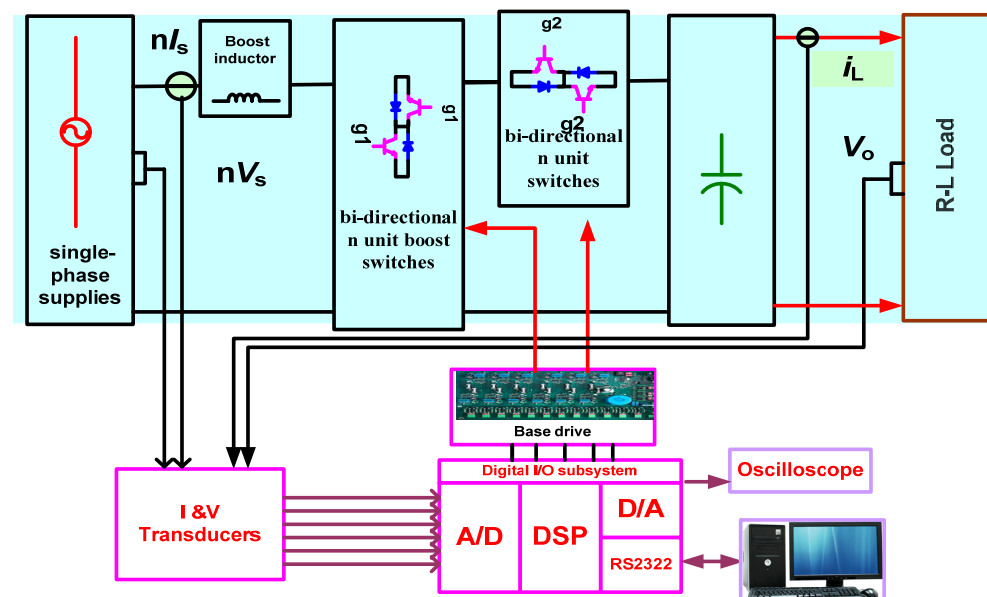


Figure 28. Block schematic of the suggested circuit's experimental setup.

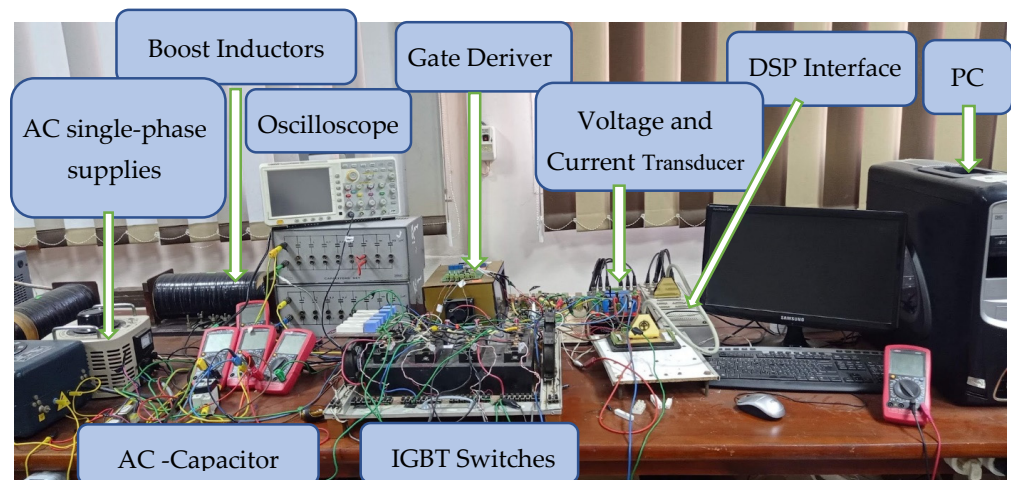


Figure 29. Hardware setup for the experimental system.

Table 3. Experimental parameters of the system.

Parameter	Symbol	Value
Supply phase voltage	$V_{s1} = V_{s2} = V_{sn}$	30 V
System frequency	F	50 Hz
Coil inductance	$L_{s1} = L_{s2} = \dots = L_{sn}$	15 mH
Coil resistance	$R_{l_{s1}} = \dots = R_{l_{s2}}$	1.4 Ω
Capacitor	C_f	5 μ F
Load resistance	R	100 Ω
Load inductance	L	80 mH
IGBT (model number)	S_{1n}, S_{2n}	CM100DY-24 H
Solid-state relays	SSR	SSR-60 VA

Steady-State Results Using Two Units

Figure 30 shows the steady-state experimental results of the proposed circuit. In the proposed practical model, two AC-to-AC converter units are used to achieve the high voltage. As shown in Figure 30, the supply current has a nearly sinusoidal waveform and is in phase with the input voltage. Figure 31 shows that the suggested control approach improves the supply current waveform by lowering the THD by up to 4.87%. Figure 32 shows the output voltage. The THD of the output voltage is shown in Figure 33. Thus, the effectiveness of the proposed circuit with the control algorithm is ensured.

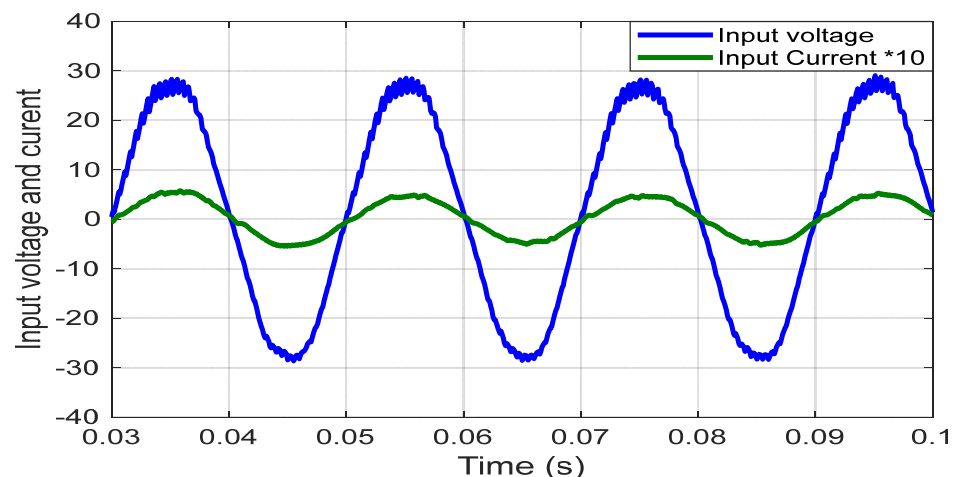


Figure 30. Input voltage and current.

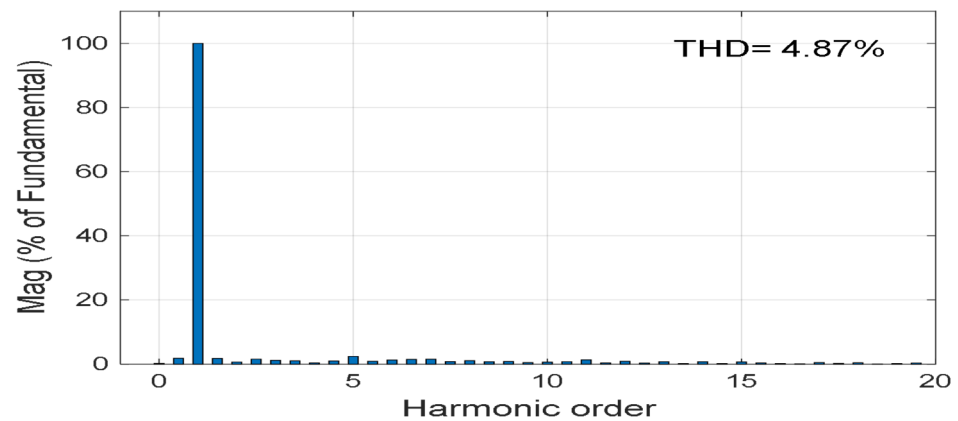


Figure 31. Harmonics spectrum of supply current.

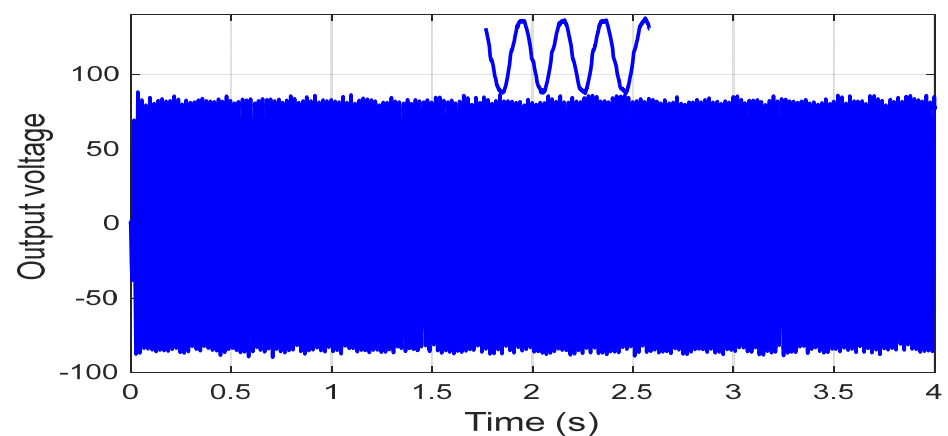


Figure 32. Output voltage for two units.

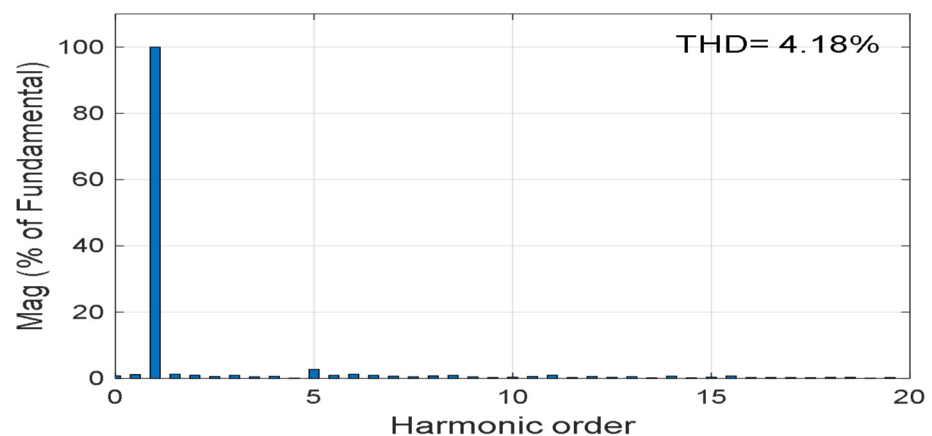


Figure 33. Harmonics spectrum of output voltage.

6. Comparison between Simulated and Experimental Results Using Three Units

This section compares the simulated results with the experimental results at the same parameter values shown in Table 3, using three units to determine the degree of convergence of the results. The results are taken under various conditions as follows:

6.1. Steady-State Results Using Three Units

Figures 34 and 35 show the load voltage of the simulated and experimental systems, respectively. These results illustrate the successful operation of the system in producing the required output voltage with precise control.

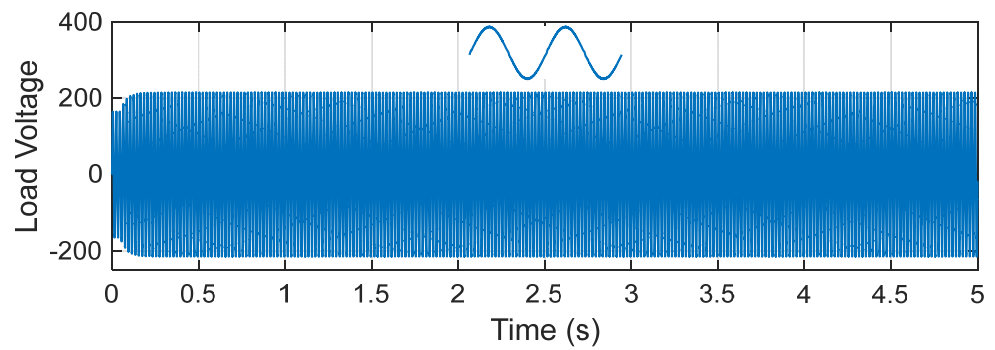


Figure 34. Load voltage for simulated system.

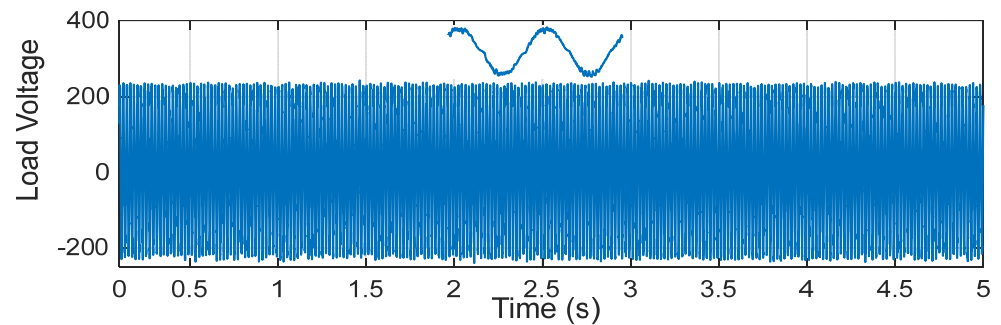


Figure 35. Load voltage for experimental system.

Figures 36 and 37 show the simulated and experimental results for the inductor current with the pulse of the bidirectional switch S_{1n} , respectively. It is evident that the switching frequency of the supply current is around 1 to 12 KHz; however, the experimental switching frequency of the supply current is about 1 to 5 KHz due to the limitations of the DSP-1104. The switch current and voltage are shown in Figures 38 and 39 for the simulated and experimental systems, respectively. These results illustrate a good agreement between the simulation and experiment.

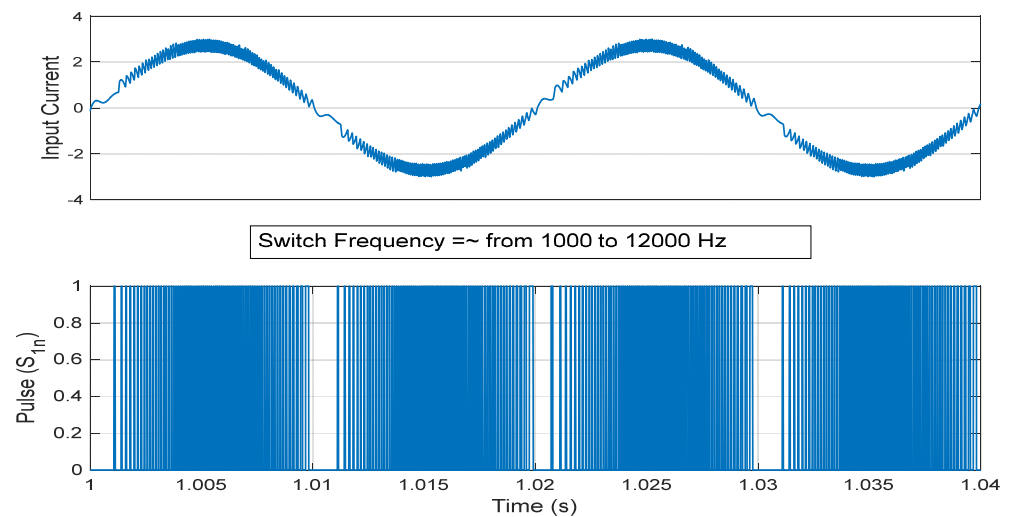


Figure 36. Simulated input current with the signal pulse (S_{1n}).

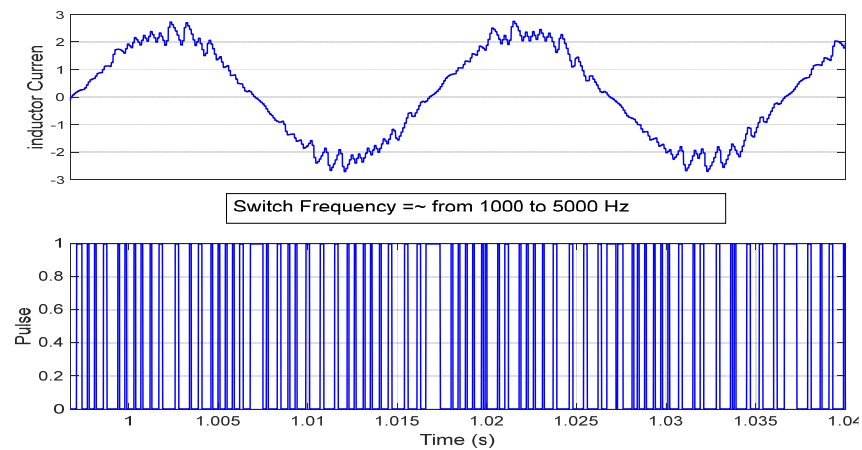


Figure 37. Experimental input current with the signal pulse (S_{1n}).

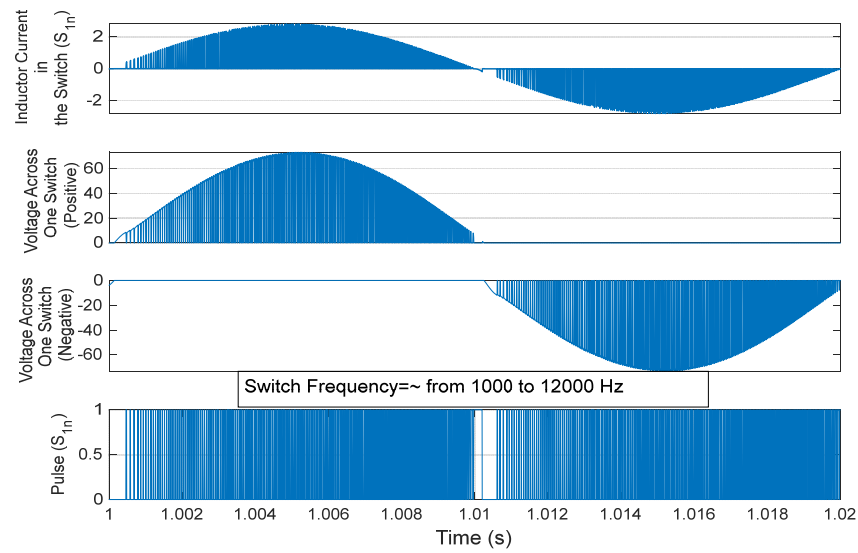


Figure 38. Simulated switch current and voltage across switch (S_{1n}) with the signal pulse.

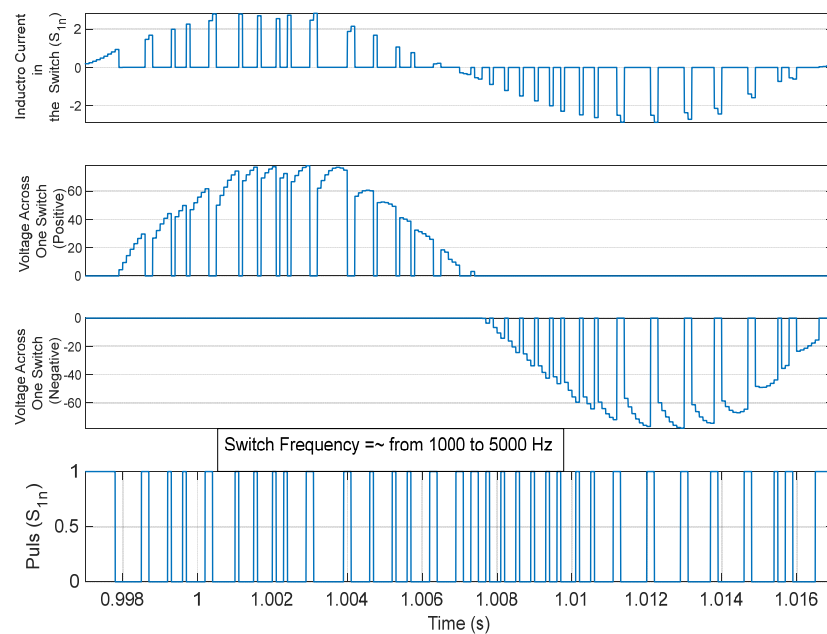


Figure 39. Experimental switch current and voltage across switch (S_{1n}) with the signal pulse.

6.2. Transient Results Using Three Units

A study is carried out to show the operation of the converter when one unit fails for one second. The simulated and experimental results for the load voltage are shown in Figures 40 and 41, respectively. The results demonstrate the capability of the control system to keep the output voltage at the required level, whether all units are working or one of them is malfunctioning.

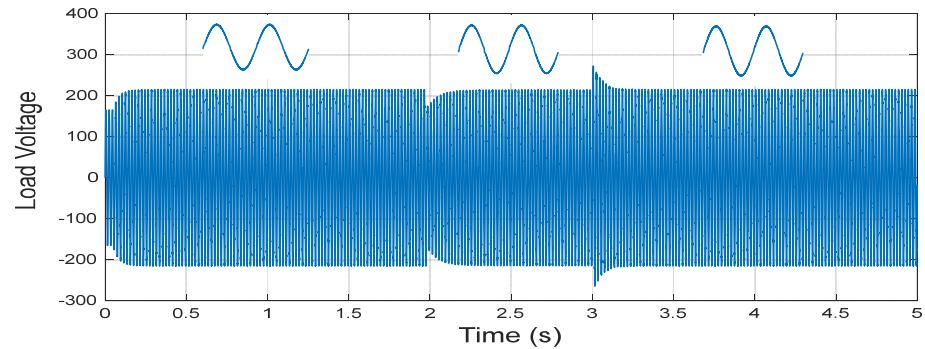


Figure 40. Simulated waveform of the load voltage.

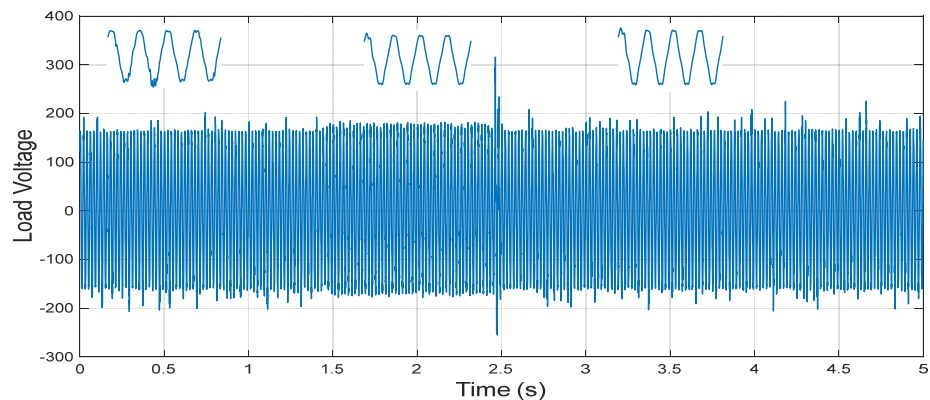


Figure 41. Experimental waveform of the load voltage.

The simulated output voltage for each of the other two working units is shown in Figure 42, while that for when the unit has stopped working is displayed in Figure 43. Figures 44 and 45 display the experimental output voltage for the other two units and for the unit that stopped working, respectively. These results illustrate the behavior of the units during a fault. It is obvious that when a problem occurs, each unit increases its output voltage to keep the load voltage constant, while the output voltage of the malfunctioning unit falls to zero.

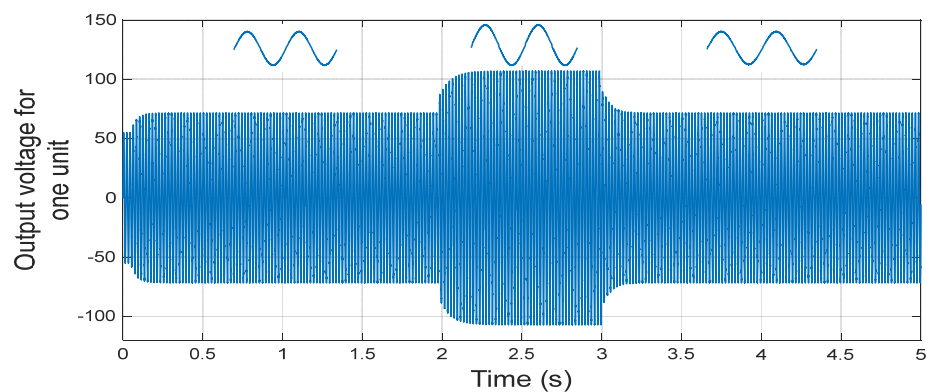


Figure 42. Simulated output voltage of one unit.

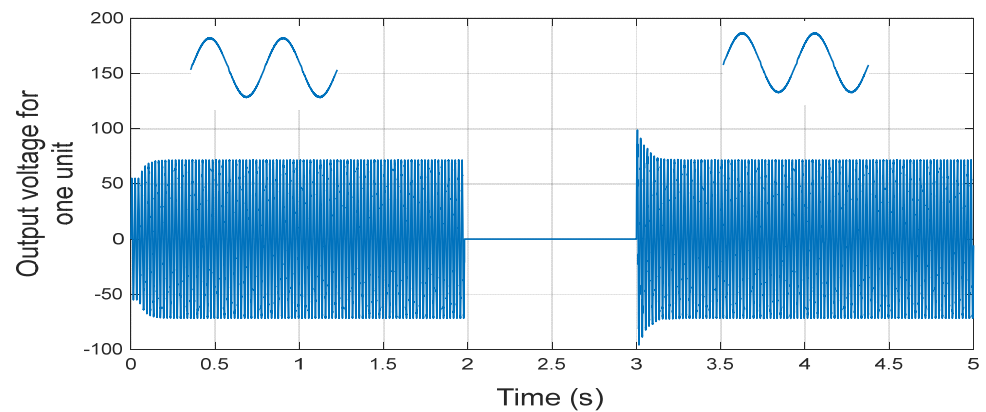


Figure 43. Simulated output voltage of stop working unit (SWU).

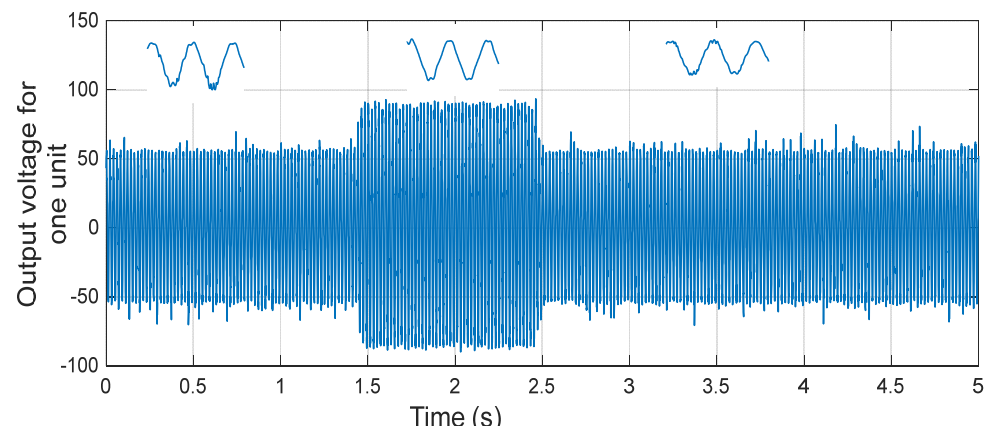


Figure 44. Experimental output voltage of one unit.

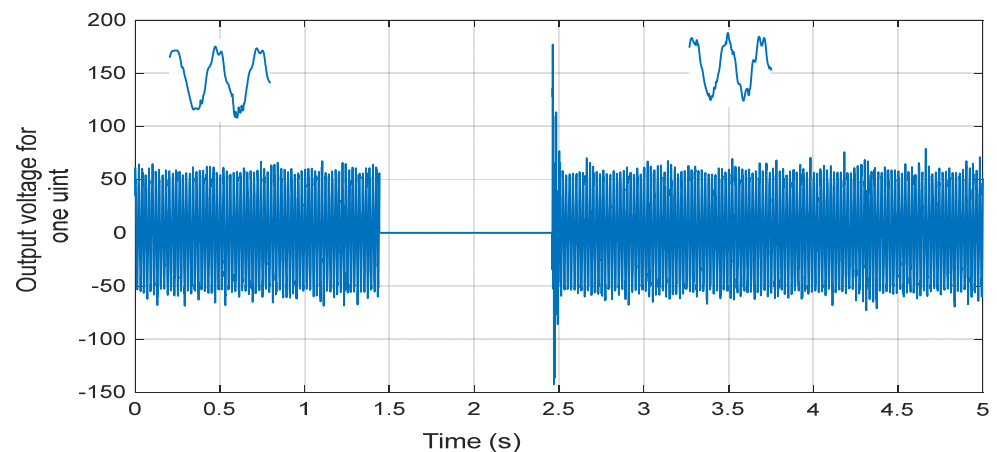


Figure 45. Experimental output voltage of stop working unit (SWU).

Figure 46 displays the simulated load current, while the experimental load current is depicted in Figure 47. It is obvious that the load current waveform is nearly sinusoidal. The input current's simulated and experimental results for the two working units are shown in Figures 48 and 49, respectively. It is obvious that when a problem occurs, each unit raises the input current for both circuits. The results demonstrate the robustness of the control system that leads to the successful operation of the system during a fault. Moreover, a good agreement between the theoretical and experimental results endorses the target circuit.

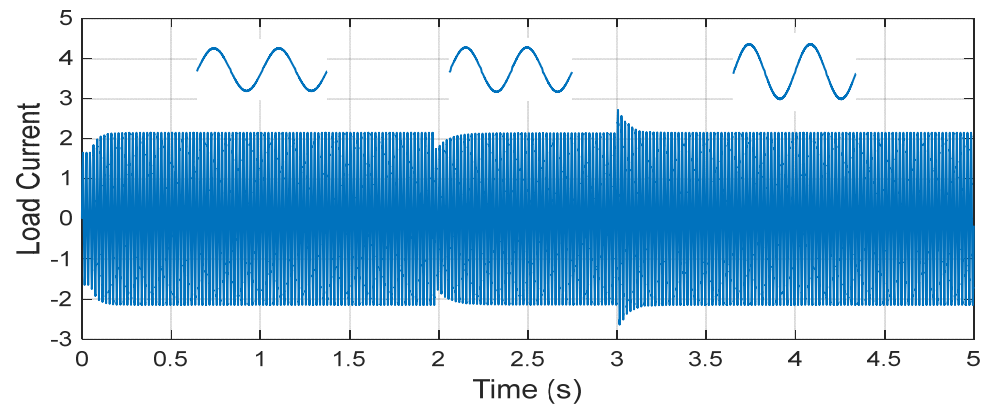


Figure 46. Simulated waveform of the load current.

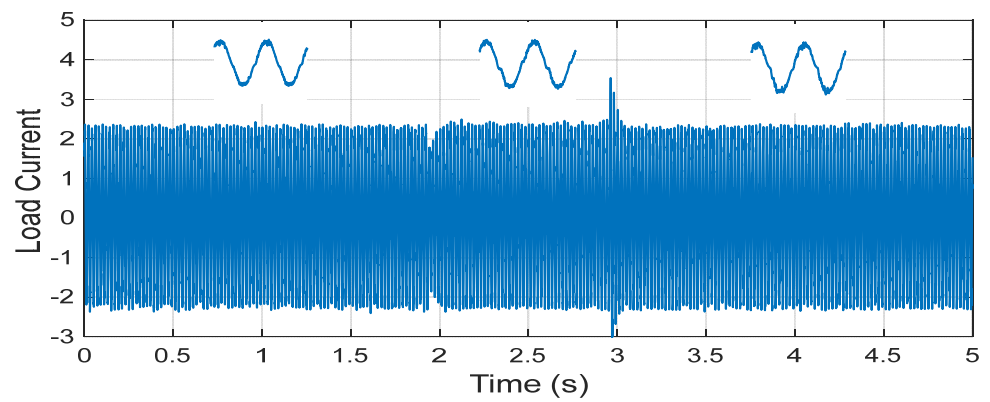


Figure 47. Experimental waveform of the load current.

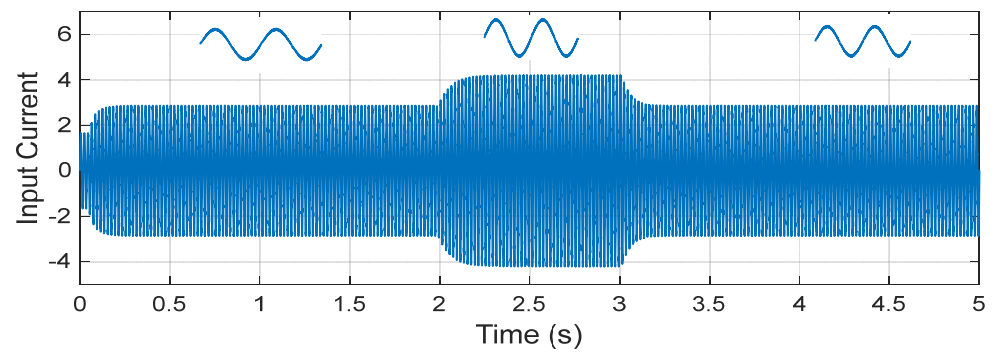


Figure 48. Simulated waveform of the input current.

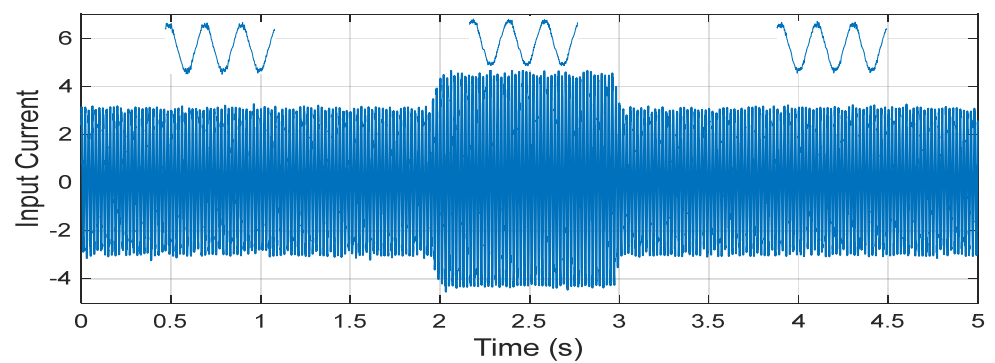


Figure 49. Experimental waveform of the input current.

Figure 50 demonstrates the theoretical and experimental relationships between the power and the input power factor for resistive and inductive loads. It is clear that the PF is close to unity and that the experimental PF value is lower than the theoretical PF value due to the frequency constraint when utilizing the DSP-1104.

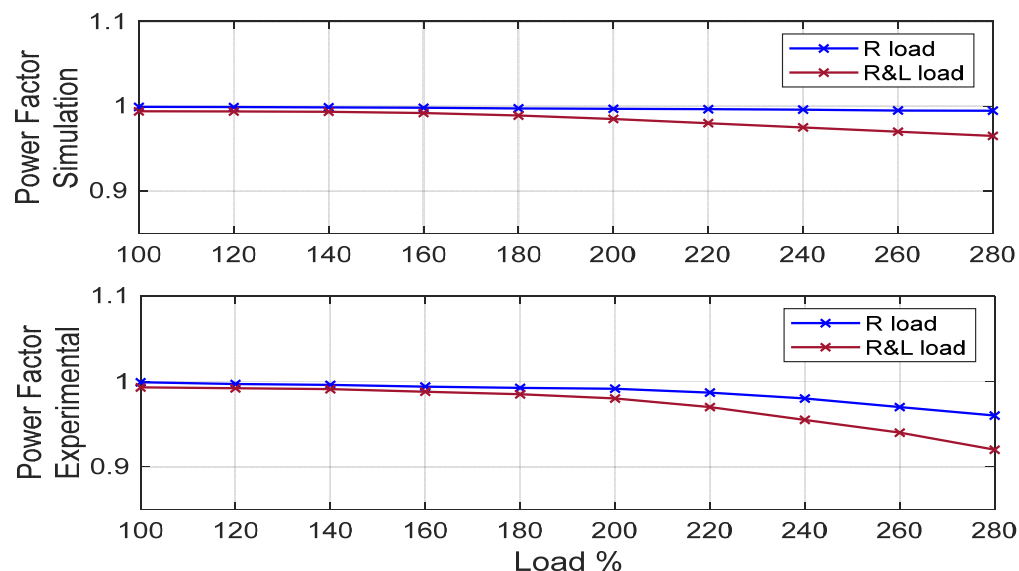


Figure 50. Power factor of simulated and experimental circuits.

7. Conclusions

In conclusion, a high-voltage-gain cascaded AC-to-AC boost converter was presented, characterized by its use of low-voltage rating semiconductor devices and a number of cascaded boost units. A simple control technique was implemented, which resulted in a significant reduction in the system size and cost. The proposed circuit was verified through a comparative assessment of the simulated and experimental results, demonstrating an excellent dynamic response with a continuous input current and a power factor close to unity. The output voltage waveform was found to be a sine wave with low harmonics, and the robustness of the control system was confirmed through a case study in which a fault occurred at one unit, showing the control circuit's ability to maintain the continuity of the output voltage. Overall, the proposed converter offers a promising solution for high-voltage-gain power-conversion applications.

Author Contributions: Conceptualization, D.S.M.O., S.M.A. and A.E.L.; methodology, D.S.M.O., S.M.A., and A.E.L.; formal analysis, D.S.M.O., S.M.A. and A.E.L.; experimental validation, D.S.M.O., S.M.A. and A.E.L.; writing—original draft, S.M.A.; writing—review and editing, D.S.M.O., S.M.A. and A.E.L. All authors have read and agreed to the published version of the manuscript.

Funding: This research received no external funding.

Institutional Review Board Statement: Not applicable.

Informed Consent Statement: Not applicable.

Data Availability Statement: Not applicable.

Conflicts of Interest: The authors declare no conflict of interest.

References

1. Liu, C.; Guo, D.; Shan, R.; Cai, G.; Ge, W.; Hu, Z. Novel Bipolar-Type Direct AC–AC Converter Topology Based on Non-Differential AC Choppers. *IEEE Trans. Power Electron.* **2019**, *34*, 9585–9599. [[CrossRef](#)]
2. Kaniewski, J.; Szczesniak, P.; Jarnut, M.; Benysek, G. Hybrid Voltage Sag/Swell Compensators: A Review of Hybrid AC/AC Converters. *IEEE Ind. Electron. Mag.* **2015**, *9*, 37–48. [[CrossRef](#)]

3. Radwan, T.S.; Lashine, A.E.; Rahman, M.A. A novel ac-ac buck-boost voltage regulator with unity input power factor. *Int. J. Electron.* **2010**, *87*, 199–210. [[CrossRef](#)]
4. da Silva Filho, O.C.; Tofoli, F.L.; Barreto, L.H.S.C.; de Souza Oliveira, D. Single-Phase Isolated AC–AC Symmetrical Full-Bridge Converter. *IEEE J. Emerg. Sel. Top. Power Electron.* **2022**, *10*, 846–855. [[CrossRef](#)]
5. Banerjee, P.K.; Raahemifar, K. AC-AC Voltage Regulation by Switch mode PWM Voltage Controller with Improved performance. *Int. J. Eng. Res. Technol.* **2013**, *2*, 2613–2619.
6. Zahra, S.; Hussainet, J.; Akram, M.M.; Siddique, M. A single-stage AC-DC-AC buck-boost converter with variable frequency operations for power quality. *Int. J. Electron. Lett.* **2021**, *9*, 355–369. [[CrossRef](#)]
7. Lee, D.; Kim, Y. Control of Single-Phase-to-Three-Phase AC/DC/AC PWM Converters for Induction Motor Drives. *IEEE Trans. Ind. Electron.* **2007**, *54*, 797–804. [[CrossRef](#)]
8. da Silva Filho, O.C.; de Almeida, B.R.; de Souza Oliveira Júnior, D.; Neto, T.R.F. High-Frequency Isolated AC–DC–AC Interleaved Converter for Power Quality Applications. *IEEE Trans. Ind. Appl.* **2018**, *54*, 4594–4602. [[CrossRef](#)]
9. Wang, Y.; Wang, P.; Cai, G.; Liu, C.; Guo, D.; Zh, H. An Improved Bipolar-Type AC–AC Converter Topology Based on Nondifferential Dual-Buck PWM AC Choppers. *IEEE Trans. Power Electron.* **2021**, *36*, 4052–4065. [[CrossRef](#)]
10. Wen, B.; Zhang, X.; Wang, Q.; Burgos, R.; Mattavelli, P.; Boroyevich, D. Comparison of three-phase ac-ac matrix converter and voltage dc-link back-to-back converter topologies based on EMI filter. In Proceedings of the 2013 IEEE Energy Conversion Congress and Exposition, Denver, CO, USA, 15–19 September 2013; pp. 2698–2706. [[CrossRef](#)]
11. Ellabban, O.; Abu-Rub, H.; Bayhan, S. Z-Source Matrix Converter: An Overview. *IEEE Trans. Power Electron.* **2016**, *31*, 7436–7450. [[CrossRef](#)]
12. Sun, Y.; Li, X.; Su, M.; Wang, H.; Dan, H.; Xiong, W. Indirect Matrix Converter-Based Topology and Modulation Schemes for Enhancing Input Reactive Power Capability. *IEEE Trans. Power Electron.* **2015**, *30*, 4669–4681. [[CrossRef](#)]
13. Nguyen, T.D.; Lee, H.-H. Dual Three-Phase Indirect Matrix Converter with Carrier-Based PWM Method. *IEEE Trans. Power Electron.* **2014**, *29*, 569–581. [[CrossRef](#)]
14. Sharifi, S.; Monfared, M.; Nikbahar, A. Highly Efficient Single-Phase Direct AC-to-AC Converter with Reduced Semiconductor Count. *IEEE Trans. Ind. Electron.* **2021**, *68*, 1130–1138. [[CrossRef](#)]
15. Ashraf, N.; Izhaet, T.; Abbas, G.; Balas, V.E.; Balas, M.M.; Lin, T.; Asad, M.U.; Farooq, U.; Gu, J. A Single-Phase Buck and Boost AC-to-AC Converter with Bipolar Voltage Gain: Analysis, Design, and Implementation. *Energies* **2019**, *12*, 1376. [[CrossRef](#)]
16. Kolar, J.W.; Friedli, T.; Rodriguez, J.; Wheeler, P.W. Review of Three-Phase PWM AC–AC Converter Topologies. *IEEE Trans. Ind. Electron.* **2011**, *58*, 4988–5006. [[CrossRef](#)]
17. Peng, F.Z.; Chen, L.; Zhang, F. Simple topologies of PWM AC-AC converters. *IEEE Power Electron. Lett.* **2003**, *1*, 10–13. [[CrossRef](#)]
18. Ursaru, O.; Lucanu, M.; Aghion, C.; Lucanu, N. Single-Phase Direct Boost AC-AC Converter. *Adv. Electr. Comput. Eng.* **2017**, *17*, 43–48. [[CrossRef](#)]
19. Lucanu, M.; Ursaru, O.; Aghion, C.; Lucanu, N. Single-Phase Direct AC-AC Boost Converter. *Adv. Electr. Comput. Eng.* **2014**, *14*, 107–112. [[CrossRef](#)]
20. Kabir, M.A.; Abedin, A.H.; Mustafiz, R.B.; Islam, M.K.; Choudhury, M.A. A single phase AC-AC boost converter with improved input power factor and THD. In Proceedings of the International Aegean Conference on Electrical Machines and Power Electronics and Electromotion, Joint Conference, Istanbul, Turkey, 8–10 September 2011; pp. 764–767. [[CrossRef](#)]
21. Khan, U.A.; Lee, J.; Park, J.-W. An Improved Cascaded Dual-Buck AC-AC Converter. In Proceedings of the 2020 IEEE 9th International Power Electronics and Motion Control Conference (IPEMC2020-ECCE Asia), Nanjing, China, 29 November–2 December 2020; pp. 1248–1253. [[CrossRef](#)]
22. Li, L.; Tang, D. Cascade Three-Level AC/AC Direct Converter. *IEEE Trans. Ind. Electron.* **2012**, *59*, 27–34. [[CrossRef](#)]
23. Kim, S.; Kim, H.-G.; Cha, H. A novel single-phase cascaded multilevel AC-AC converter without commutation problem. In Proceedings of the 2014 IEEE Energy Conversion Congress and Exposition (ECCE), Pittsburgh, PA, USA, 14–18 September 2014; pp. 556–562. [[CrossRef](#)]
24. Khan, A.A.; Cha, H.; Baek, J.; Kim, J.; Cho, J. Cascaded Dual-Buck AC–AC Converter with Reduced Number of Inductors. *IEEE Trans. Power Electron.* **2017**, *32*, 7509–7520. [[CrossRef](#)]
25. Ahmed, H.F.; El Moursi, M.S.; Zahawi, B.; Al Hosani, K. A High-Frequency Isolated Multilevel Cascaded-Type Bipolar Direct PWM AC–AC Converter for Utility Voltage Compensation. *IEEE Trans. Ind. Appl.* **2021**, *57*, 3188–3201. [[CrossRef](#)]
26. Ahmed, H.; Çelik, D. Sliding mode based adaptive linear neuron proportional resonant control of Vienna rectifier for performance improvement of electric vehicle charging system. *J. Power Sources* **2022**, *542*, 231788. [[CrossRef](#)]
27. Middlebrook, R.D.; Cuk, S. A general unified approach to modelling switching-converter power stages. In Proceedings of the 1976 IEEE Power Electronics Specialists Conference, Cleveland, OH, USA, 8–10 June 1976; pp. 18–34. [[CrossRef](#)]
28. Sun, J.; Grotstollen, H. Averaged modelling of switching power converters: Reformulation and theoretical basis. In Proceedings of the PESC'92 Record. 23rd Annual IEEE Power Electronics Specialists Conference, Toledo, Spain, 29 June–3 July 1992; Volume 2, pp. 1165–1172. [[CrossRef](#)]

29. Sun, J.; Grotstollen, H. Symbolic analysis methods for averaged modeling of switching power converters. *IEEE Trans. Power Electron.* **1997**, *12*, 537–546. [[CrossRef](#)]
30. Lashine, A.E.; Osheba, M.S.; Mansour, A.S. Stability Analysis and Performance Evaluation of a Multifunction Converter. *Eng. Res. J.* **2021**, *44*, 125–134. [[CrossRef](#)]

Disclaimer/Publisher’s Note: The statements, opinions and data contained in all publications are solely those of the individual author(s) and contributor(s) and not of MDPI and/or the editor(s). MDPI and/or the editor(s) disclaim responsibility for any injury to people or property resulting from any ideas, methods, instructions or products referred to in the content.